Magnetic Resonance Imaging Visualization of Hyaluronidase in Ovarian Carcinoma

Liora Shiftan,[1] Tomer Israely,[1] Miriam Cohen,[2] Veronica Frydman,[3] Hagit Dafni,[1] Robert Stern,[4] and Michal Neeman[1]

Departments of [1]Biological Regulation, [2]Molecular Cell Biology, and [3]Chemical Research Support, The Weizmann Institute of Science, Rehovot, Israel and [4]Department of Pathology, School of Medicine, University of California at San Francisco, San Francisco, California

Abstract

Hyaluronan, a high molecular weight, negatively charged polysaccharide, is a major constituent of the extracellular matrix. High molecular weight hyaluronan is antiangiogenic, but its degradation by hyaluronidase generates proangiogenic breakdown products. Thus, by expression of hyaluronidase, cancer cells can tilt the angiogenic balance of their microenvironment. Indeed, hyaluronidase-mediated breakdown of hyaluronan correlates with aggressiveness and invasiveness of ovarian cancer metastasis and with tumor angiogenesis. The goal of this work was to develop a novel smart contrast material for detection of hyaluronidase activity by magnetic resonance imaging (MRI). Gadolinium-diethylenetriaminepentaacetic acid (GdDTPA) covalently linked to hyaluronan on the surface of agarose beads showed attenuated relaxivity. Hyaluronidase, either purified from bovine testes or secreted by ES-2 and OVCAR-3 human epithelial ovarian carcinoma cells, activated the hyaluronan-GdDTPA-beads by rapidly altering the R_1 and R_2 relaxation rates. The change in relaxation rates was consistent with the different levels of biologically active hyaluronidase secreted by those cells. Hyaluronan-GdDTPA-beads were further used for demonstration of MRI detection of hyaluronidase activity in the proximity of s.c. ES-2 ovarian carcinoma tumors in nude mice. Thus, hyaluronan-GdDTPA-beads could allow noninvasive molecular imaging of hyaluronidase-mediated tilt of the peritumor angiogenic balance. (Cancer Res 2005; 65(22): 10316-23)

Introduction

Hyaluronan, also known as hyaluronate or hyaluronic acid, is a high molecular weight linear glycosaminoglycan composed of repeating disaccharides of glucuronic acid and *N*-acetylglucosamine. Hyaluronan is an important structural element in cartilage, synovial fluid, skin of vertebrates, and vitreous humor of the eye (1). Hence, hyaluronan plays an important role in maintenance of intact architecture in normal tissues; it absorbs a large volume of water and creates a gel-like environment. Hyaluronan affects physiologic and pathologic processes that require cell movement, such as tissue organization and morphogenesis, wound healing, inflammation, angiogenesis, and tumor metastasis.

High molecular weight hyaluronan is degraded by hyaluronidase. Low molecular weight degradation products are known to stimulate endothelial cell proliferation and promote neovasculariza-tion, whereas the intact high molecular weight hyaluronan is antiangiogenic (2). Hyaluronidase was first identified in 1928 as a "spreading factor" of viral agents and was later characterized as hyaluronan-degrading enzyme and named hyaluronidase (3–5). Hyaluronidase activity is high in necrotic tumors and elevated in the sera of cancer patients (6).

Six hyaluronidase-like genes, coding for different enzymes with varying substrate specificities, based on their enzymatic activity and optimal pH for activity are identified in mammals (7). The main hyaluronidases that were studied are hyaluronidase-1, hyaluronidase-2, and PH-20. Hyaluronidase-1, the major hyaluronidase found in the plasma and urine is a 57-kDa protein composed of a single peptide chain of 49 kDa, with ∼8 kDa of posttranslational glycosylation. Hyaluronidase-1 is also a lysosomal enzyme that can cleave hyaluronan to small tetrasaccharides and disaccharides (8) and has ∼40% identity to the enzyme PH-20 found mainly in sperm (7). Hyaluronidase-1 is also known as LUCA-1 defined by functional tumor suppressor activity (9). The activity of hyaluronidase-1 in the serum is suppressed by IαI, a potent inhibitor of hyaluronidase (10).

Hyaluronidase-2 is generally anchored to the plasma membrane by a glycosylphosphatidylinositol link. It cleaves high molecular weight hyaluronan to ∼20-kDa fragments (50 disaccharides), which are proangiogenic. Hyaluronidase-2 overexpression accelerates tumor formation of murine astrocytoma cells (11) but can also accelerate apoptosis (12). It seems that both hyaluronidase-1 and hyaluronidase-2 can function either as oncogene or as tumor suppressor gene product. Secretion of hyaluronidase by cancer cells can contribute to their aggressiveness and invasiveness. Thus, hyaluronidase provides the intermediate hyaluronan fragments that induce angiogenesis (13). Moreover, secretion of hyaluronidase by the cancer cell enables digestion of the hyaluronan barrier and thus facilitates invasion of tumor cells to neighboring organs and tissues. It is reported that hyaluronidase activity in ovarian cancer tissue is significantly higher than in endometrial cancer tissue. A significant correlation is found between hyaluronidase activity and metastasis of ovarian cancer (14). Moreover, treatment of conditioned medium with hyaluronidase increases the adhesion of ovarian cancer tumor cells to mesothelial monolayer that serves as a model for metastatic dissemination in the peritoneal cavity (15). Because hyaluronan, hyaluronidase, and CD44 (hyaluronan receptor) are involved in the progression of ovarian carcinoma (16–19), noninvasive detection of the presence and activity of hyaluronidase may give indication for the process and presence of metastasis.

Several methods are used for the detection of hyaluronidase, including quantitative spectroscopic ELISA-like assay (20), a microtiter-based assay for hyaluronidase activity (21), the Morgan-Elson reaction (22) and its fluorimetric version (23),

chromatography (24), and particle exclusion assay (25). However, none of these methods can be applied *in vivo* for noninvasive imaging.

The goal of this work was to develop a novel method for the detection of hyaluronidase by magnetic resonance imaging (MRI). A new contrast material was constructed by linking of gadolinium-diethylenetriaminepentaacetic acid (GdDTPA)–tagged hyaluronan to nontoxic agarose beads. We report here that hyaluronidase secreted by ovarian carcinoma cells caused significant activation of the contrast material, manifested by alternations in R_1 and R_2 relaxation rates, *in vitro* as well as in the surrounding of s.c. ovarian tumor xenografts. Because hyaluronidase activity is correlated with the progression and metastatic spread of ovarian carcinomas to the peritoneum, this method could potentially be further developed for clinical molecular imaging of hyaluronidase.

Materials and Methods

Synthesis of hyaluronan-gadolinium-diethylenetriaminepentaacetic acid-beads. Hyaluronan-GdDTPA was synthesized as described (26). Briefly, hyaluronan (50 mg, extracted from human umbilical cord; Sigma Chemical Co., St. Louis, MO) was dissolved in MES (0.1 mol/L, 50 mL, pH 4.75, Sigma). The carboxyl groups of hyaluronan were activated by addition of *N*-(3-dimethylaminopropyl)-*N*-ethylcarbodiimide hydrochloride (EDC; 2.4 mg) followed by addition of ethylenediamine (2 mg) and stirring overnight at room temperature. The product was purified by dialysis against double-distilled water, reacted with DTPA dianhydride (18.7 mg, Sigma), and dissolved in filtered DMSO (55 mL) overnight at room temperature. After second dialysis, gadolinium (III) chloride (23.5 mg, Sigma) in double-distilled water was added, the mixture was stirred for 24 hours, and a third dialysis was done. Gadolinium content in the end product was measured by inductively coupled plasma-mass spectrometry (ICP-MS) showing $\sim$0.018 mg gadolinium bound to 1 mg hyaluronan (i.e., a ratio of 1:17 between gadolinium and hyaluronan disaccharides, respectively). The product was lyophilized and stored at room temperature in a desiccator and was reconstituted to a working concentration in double-distilled water.

Hyaluronan-GdDTPA was further covalently bound to avidin-agarose beads (bead size, 0.040-0.165 mm; Sigma). Avidin-linked agarose beads (50 μL bead suspension containing $\sim$6 × 10^{-9} mol avidin; Sigma) were mixed with 5-(biotinamido)pentylamine (2 μg; Pierce Biotechnology, Rockford, IL) in MES (pH 5.5, 0.1 mol/L) at room temperature to let the biotin in the 5-(biotinamido)pentylamine link to the avidin on the agarose beads. The carboxyl groups of hyaluronan (25 mg hyaluronan-GdDTPA) were activated in MES by EDC (2 mg) and added to the 5-(biotinamido)-pentylamine–conjugated beads, stirred at room temperature overnight, and purified by dialysis against double-distilled water. In contrast with the source agarose beads, hyaluronan-GdDTPA-beads are highly hydrated and generate a clear and stable suspension, whereas the native agarose beads are nontransparent and tend to settle rapidly.

Synthesis of hyaluronan-Bodipy. Hyaluronan-Bodipy was synthesized as described previously (27) and purified by dialysis.

Cell culture. Human epithelial ovarian carcinoma cell lines ES-2 and OVCAR-3 (kindly provided by Prof. Steffen Hauptmann, Institute of Pathology, Rudolf-Virchow-Haus, Berlin, Germany) were cultured in DMEM supplemented with 10% FCS. Chondrocytes (RCJ-P, rat chondrocytes from fetal calvaria, batch 15.01.98; Prochon Biotec Ltd., Rehovot, Israel) were cultured in α-MEM supplemented with 15% FCS. All media were supplemented with 100 units/mL penicillin, 0.1 mg/mL streptomycin, 0.06 mg/mL amphotericin, and 0.292 mg/mL L-glutamine.

Particle exclusion assay. The very thick hyaluronan coat of the chondrocytes (typically $\sim$4.4 ± 0.7 μm; ref. 28) was used here as the substrate for analysis of its degradation by hyaluronidase-containing samples. Chondrocytes were grown to confluence in 10-cm culture dish,

harvested, diluted 1:100, and seeded on a particle exclusion assay plate (35-mm culture dish with 14-mm microwell; MatTek, Ashland, MA). After overnight incubation, the medium was replaced by fresh medium, hyaluronidase in PBS, or by conditioned medium removed from different ovarian carcinoma cell lines for incubation of 1 hour in 37°C. This incubation allowed hyaluronidase in the different treatments to degrade the hyaluronan layer around the chondrocytes. After incubation, the medium was replaced by human RBC type O (Sigma) diluted in DMEM. The RBC are excluded from the hyaluronan around the chondrocytes and are used here to delineate the border of hyaluronan, which is a transparent gel, allowing it to become visualized by light microscopy. Samples were viewed in visible light using an Axioskop microscope (Zeiss, Oberkochen, Germany). Images were acquired using a scientific-grade cooled charged-coupled device camera (Model CC350, Photometrics Co., Tucson, AZ). The experiment was repeated five times, and in each, at least five cells from a particular treatment were measured.

Reverse transcription-PCR. Total RNA was extracted using TRI-Reagent (Molecular Research Center, Inc., Cincinnati, OH) according to the manufacturer's instruction and reverse transcribed in 20 μL volume using RNase reverse transcriptase (SuperScript II, Invitrogen/Life Technologies, Inc., Carlsbad, CA) with 180 pmol hexamer random primer. Aliquots (2 μL) of the reverse transcription products were used for PCR. The following sense and antisense primers were used: hyaluronidase-2 sense 5′-GCTCAAGCCCACAGCACCAC-3′ and antisense 5′-CAGTGTCTCCAG-CATGAACTGC-3′ and hyaluronidase-1 sense 5′-CACCGTCTGGAATG-CAAACA-3′ and antisense 5′-GTTGGCTACCACATCGAAGACA-3′ (29). PCR variables were as follows: hyaluronidase-1, 94°C for 3 minutes, 31 cycles of 94°C for 20 seconds, 58°C for 30 seconds, and 72°C for 45 seconds followed by 72°C for 3 minutes; hyaluronidase-2, 94°C for 3 minutes, 24 cycles of 94°C for 20 seconds, 60°C for 30 seconds, and 72°C for 45 seconds followed by 72°C for 3 minutes. S16 was used for internal control: 5′-CGTTCACCTTGATGAGCCCAT-3′ and 5′-TCCAAGGGTCCGCTGCAGTC-3′.

Western blotting analysis. Confluent ovarian carcinoma cells OVACR-3 and ES-2 were washed with serum-free DMEM and incubated in serum-free medium for 24 or 48 hours. The medium was collected, centrifuged to remove cells, and concentrated using Amicon Ultra 10,000 MWCO (Millipore, Bedford, MA). Concentrated media were electrophoresed (12% SDS-polyacrylamide gel). Blocked membranes [5% milk in TBS-Tween 20 (TBST), 1 hour, room temperature] were incubated overnight at 4°C with either anti-hyaluronidase-1 or anti-hyaluronidase-2 polyclonal antibody (diluted 1:1,000, produced by Prof. R. Stern). Membranes were washed thrice with TBST and incubated with horseradish peroxidase–labeled antibodies (1:10,000; Zymed, Inc., San Francisco, CA). The immunoreactive bands were detected by commercial enhanced chemiluminescence (Santa Cruz Biotechnology, Santa Cruz, CA). The intensity of the signal was quantified by computerized densitometry (Quantity One, Bio-Rad, Hercules, CA).

Immunofluorescent cell staining. Polyclonal antibodies against hyaluronidase-1 and hyaluronidase-2 were kindly provided by R. Stern. Antibodies were prepared in rabbits using synthetic peptides from hyaluronidase-1 and hyaluronidase-2, corresponding to amino acids 104 to 120 and 100 to 116, respectively, as described previously (30). Cells seeded on 18-mm coverslips were cultured to confluence, washed twice in PBS, and fixed in 2.5% paraformaldehyde for 20 minutes in room temperature. Following three washes in PBS, the cells were permeabilized in 0.2% Triton (Sigma) in PBS and washed again. The coverslips were incubated with anti-hyaluronidase-1 or anti-hyaluronidase-2 antibody (diluted 1:200) for 1.5 hours at room temperature. Following three washes with PBS, the coverslips were incubated with secondary antibody (goat anti-rabbit FITC, Jackson ImmunoResearch, West Grove, PA) followed by 4′,6-diamidino-2-phenylindole (DAPI) nuclear staining (Sigma, 1:100). In control sections, only the secondary antibody was used.

Ovarian carcinoma tumor xenografts. All animal experiments were approved by the Institutional Animal Care and Use Committee.

CD-1 female nude mice 12 weeks old were inoculated with 3 × 10^6 ES-2 cells. MRI studies were done 3 weeks after inoculation. The mice

were anesthetized with i.p. ketamine (75 mg/kg; Ketaset, Fort Dodge Laboratories, Fort Dodge, IA) and xylazine (3 mg/kg; XYL-M, VMD, Arendonk, Belgium). A vein flow (24GA, BD Neoflon, Becton Dickinson, Helsingborg, Sweden) was inserted s.c. for local administration of hyaluronan-GdDTPA-beads (5 mg/mL).

***In vitro* magnetic resonance imaging studies.** Hyaluronan-GdDTPA-beads (1 mg/mL) were incubated with hyaluronidase for 15 minutes at 37°C. The enzyme used was either bovine testes hyaluronidase (Sigma, type IV-S from bovine testes, 0.3 mg/mL) or hyaluronidase secreted to the conditioned medium of ovarian carcinoma cell lines.

MRI measurements were done on a 400-MHz (9.4 T) vertical wide-bore DMX spectrometer equipped with a microimaging attachment with a 5-mm Helmholtz radiofrequency coil or on a horizontal 4.7 T Biospec (Bruker, Karlsruhe, Germany). For R_2 measurements, multiecho spin echo sequence was used to acquire eight consecutive echoes with interecho spacing of 10 ms [echo time (TE) 10, 20, 30, 40, 50, 60, 70, and 80 ms, repetition time (TR) 2,000 ms, two averages, field of view (FOV) 1 × 1 cm, slice thickness 1 mm, matrix 128 × 128, spectral width 50,000 Hz]. For R_1 measurements, spin echo images were acquired at eight different TRs ranging between 2,000 and 200 ms (two averages, FOV 1 × 1 cm, slice thickness 1 mm, matrix 128 × 128, spectral width 50,000 Hz).

For the kinetic analysis, the sample was equilibrated to 37°C within the spectrometer before the beginning of the measurements. R_2pre was measured and the enzyme was injected to the test tube through a catheter and R_2post was measured.

***In vivo* magnetic resonance imaging measurements.** MRI experiments were done on a horizontal 4.7 T Biospec spectrometer using an actively radiofrequency decoupled 1.5 cm surface coil embedded in a Perspex board and a birdcage transmission coil. Anesthetized mice were placed supine with the graft located above the center of the surface coil. The mice were immobilized using adhesive tape and covered with a paper blanket to reduce temperature drop during the measurement. For R_2 measurements, multiecho spin echo images were acquired with TR 500 ms, TE 10 to 80 ms, slice thickness 1 mm, and FOV 3.5 × 3.5 cm. For R_1 measurements, a series of T_1-weighted three-dimensional gradient-echo images, with pulse flip angles of 5°, 15°, 30°, 50°, and 70°, were acquired to determine the R_1 relaxation rate before administration of the contrast material. Variables were as follows: TR 10 ms, TE 3.561 ms, two averages, spectral width 50,000 Hz, FOV 3.5 × 3.5 × 1.75 cm (obtained by acquisition using an actively decoupled surface coil), matrix 128 × 128 × 64, zero filled to 128 × 128 × 128. Consecutive postcontrast T_1-weighted three-dimensional gradient-echo images were acquired 2 to 30 minutes after the contrast agent was administered (pulse flip angle 15°).

Analysis of the magnetic resonance imaging data. MRI data were analyzed on a personal computer using Matlab (The Math Works, Inc., Natick, MA). Images acquired with eight different TE values were used for generation of R_2 maps by nonlinear least-square pixel-by-pixel fitting to a single exponent (Eq. A):

$$I = Ae^{-TE*R_2} \tag{A}$$

where I is the measured signal intensity for each TE and A is the fitted steady-state signal intensity in fully relaxed images. R_2 values within a region of interest were averaged and SD was calculated.

R_1 relaxation rates for the *in vitro* experiments were derived by non-linear single exponential fitting of images acquired at different TRs (Eq. B):

$$I = A(1 - Be^{-TR*R_1}) \tag{B}$$

where I is the measured signal intensity for each TR. A, B, and R_1 were derived from optimization of the curve fitting; A is the steady-state signal intensity in fully relaxed images and B is ~ 1 for steady-state saturation.

R_1pre maps for the *in vivo* experiments were derived by a nonlinear best fit to Eq. C:

$$I = \frac{M_0 \sin \alpha (1 - e^{-TR \bullet R_1 pre})}{1 - \cos \alpha \bullet e^{-TR \bullet R_1 pre}} \tag{C}$$

where I is the signal intensity as a function of the pulse flip angle α; TR = 10 ms; the pre-exponent term, M_0, includes the spin density and the T_2 relaxation, which are assumed to be constant. A single R_1 value was derived for each voxel (31). Postcontrast R_1 values (R_1post) were calculated from precontrast and postcontrast three-dimensional gradient-echo signal intensities (Eq. D):

$$\frac{I_{pre}}{I_{post}} = \frac{M_0 \sin \alpha (1 - e^{-TR \bullet R_1 pre})/(1 - \cos \alpha \bullet e^{-TR \bullet R_1 pre})}{M_0 \sin \alpha (1 - e^{-TR \bullet R_1 post})/(1 - \cos \alpha \bullet e^{-TR \bullet R_1 post})} \tag{D}$$

Results

Hyaluronan-gadolinium-diethylenetriaminepentaacetic acid-beads as novel contrast material for detection of hyaluronidase by magnetic resonance imaging. Particles presenting local high concentration of hyaluronan, serving as MRI detectable substrate for hyaluronidase, were generated by cross-linking hyaluronan-GdDTPA to agarose beads (Fig. 1A). The product, hyaluronan-GdDTPA-beads, contained $\sim 1.8\%$ (w/w) gadolinium as determined by ICP-MS. The specific R_1 relaxivity of the hyaluronan-GdDTPA-beads was measured to be 11 mmol/L^{-1} s^{-1} per gadolinium, and the R_2 relaxivity of the hyaluronan-GdDTPA-beads was measured to be 25 mmol/L^{-1} s^{-1} per gadolinium (Fig. 1B). To check whether chemical modification of hyaluronan can still be recognized and cleaved by hyaluronidase, we used a fluorescently tagged hyaluronan. Hyaluronan-Bodipy incubated with bovine testes hyaluronidase or double-distilled water was loaded on Sephadex G-25 columns and eluted with double-distilled water. Aliquots were collected from the two columns and fluorescence was measured at 538 nm (Fig. 2A). The undigested hyaluronan-Bodipy was eluted with the void volume, whereas the hyaluronan-Bodipy that was incubated with hyaluronidase showed delayed elution of the lower molecular weight degradation products. Hence, the modification of hyaluronan did not prevent the ability of hyaluronidase to recognize and cleave it.
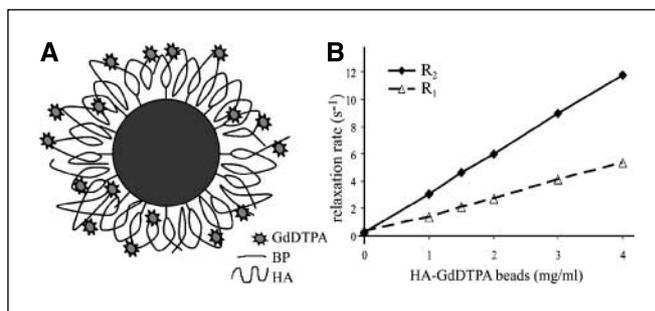
Figure 1. Hyaluronan-GdDTPA-beads as contrast material for MRI detection of hyaluronidase. *A,* scheme of the contrast material. Hyaluronan (*HA*) was conjugated with GdDTPA, and the complex was attached to agarose-avidin beads via 5-(biotinamido)pentylamine (*BP*) as a linker. Degradation of the hyaluronan in the contrast material by hyaluronidase to lower molecular weight fragments was expected to alter R_1 and R_2 relaxivity and thus change the contrast in MRI. *B,* measurement of the R_1 and R_2 relaxivity of hyaluronan-GdDTPA-beads. The R_1 relaxivity was 1.3 mL mg^{-1} s^{-1} (11 mmol/L^{-1} s^{-1} per gadolinium), and the R_2 relaxivity was 2.9 mL mg^{-1} s^{-1} (25 mmol/L^{-1} s^{-1} per gadolinium).
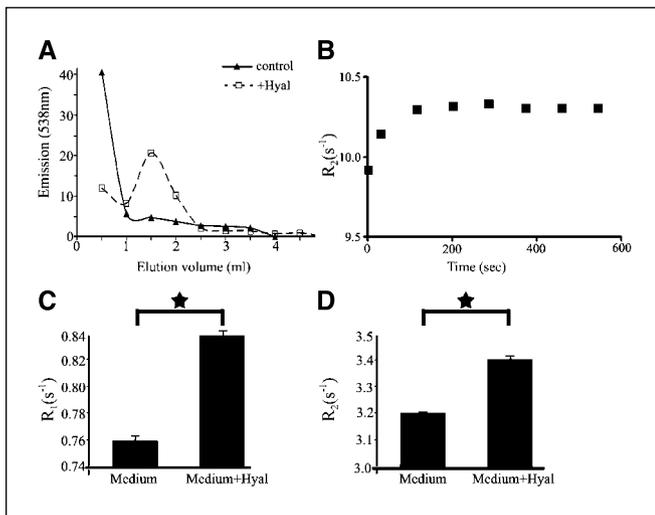
Figure 2. Hyaluronidase activity in degradation of chemically modified hyaluronan. *A,* detection of hyaluronidase (*Hyal*) activity by fluorescence. Fluorescence of aliquots of hyaluronan-Bodipy treated (□) or untreated (▲) with bovine testes hyaluronidase that was run through a column. Binding the Bodipy to the hyaluronan did not affect the ability of hyaluronidase to digest hyaluronan. *B,* MRI detection of the kinetics of degradation of hyaluronan-GdDTPA-beads by bovine testes hyaluronidase. The enzyme was injected into 37°C preheated nuclear magnetic resonance tube and changes in R_2 were measured. The changes in R_2 were rapid and reached plateau within a few minutes. *C* and *D,* detection of hyaluronidase activity by MRI. R_1 and R_2 relaxation rates of FCS-containing medium in the absence (*left*) or presence (*right*) of hyaluronidase. Relaxation rates were measured after incubation with hyaluronan-GdDTPA-beads (1 mg/mL) for 15 to 30 minutes at 37°C ($n = 6$; two-tailed unpaired *t* test; $P < 0.009$).

Hyaluronan-gadolinium-diethylenetriaminepentaacetic acid-beads allow detection of hyaluronidase activity by magnetic resonance imaging. Suspension of hyaluronan-GdDTPA-beads in culture medium (plus 15% FCS) was used to test the ability of MRI to detect hyaluronidase-dependent changes in R_1 and R_2 relaxation rates of water (Fig. 2C and D). The R_1 measured for hyaluronan-GdDTPA-beads incubated with bovine testes hyaluronidase in serum-containing medium was 0.84 s^{-1} (15 minutes at 37°C). This was significantly higher relative to control hyaluronan-GdDTPA-beads suspended in medium without hyaluronidase that had R_1 of 0.75 s^{-1} ($n = 6$; two-tailed unpaired *t* test; $P < 0.009$; Fig. 2C). The R_2 measured for hyaluronan-GdDTPA-beads incubated with bovine testes hyaluronidase in serum-containing medium was 3.4 s^{-1}, this was significantly higher relative to control hyaluronan-GdDTPA-beads suspended in medium without hyaluronidase that had R_2 of 3.2 s^{-1} ($n = 6$; two-tailed unpaired *t* test; $P < 0.009$; Fig. 2D). The rate of the enzymatic reaction was measured by injecting hyaluronidase into preheated tube (37°C) that contained hyaluronan-GdDTPA-beads and measuring the changes in R_2. The enzymatic reaction was quite rapid and was over within few minutes (Fig. 2B).

Activity of hyaluronidase secreted by human epithelial ovarian carcinoma cells. Particle exclusion assay was used to evaluate the biological activity of hyaluronidase secreted by two human epithelial ovarian carcinoma cell lines, OVCAR-3 and ES-2 (Fig. 3A-E). The chondrocytes used in this assay produce a thick pericellular coat composed of high molecular weight hyaluronan. RBC, which are added to the culture plate, are excluded by the hyaluronan layer, thereby delineating it and allowing its visualization (Fig. 3A). After addition of commercial hyaluronidase, the

high molecular weight hyaluronan is degraded, allowing the RBC to approach the chondrocyte membrane (Fig. 3B). The activity of hyaluronidase in medium conditioned by OVCAR-3 and ES-2 cells was examined by addition of this medium to the chondrocytes (Fig. 3C and D, respectively). Conditioned medium from ES-2 cells but not from OVCAR-3 cells degraded the hyaluronan layer, showing a significantly higher activity of hyaluronidase that is secreted to the culture medium by ES-2 cells ($n = 5$; two-tailed unpaired *t* test; $P = 0.02$; Fig. 3E).

Expression and secretion of hyaluronidase-1 and hyaluronidase-2 by ovarian carcinoma cells. The expression of hyaluronidase-1 and hyaluronidase-2 was measured in the two human epithelial ovarian carcinoma cell lines, OVCAR-3 and ES-2, using reverse transcription-PCR (RT-PCR) analysis. No significant differences in the mRNA levels of hyaluronidase-1 and hyaluronidase-2 were detected between the two cell lines (Fig. 3F and G). The cells were also stained with anti-hyaluronidase-1 and anti-hyaluronidase-2 antibodies (Fig. 4). Those staining showed that the amount of intracellular hyaluronidase-1 and hyaluronidase-2 in OVCAR-3 and ES-2 cells was similar. In contrast to the similarity in hyaluronidase mRNA expression levels and the immunohistochemistry, a large difference was detected in the amount of hyaluronidase secreted by OVCAR-3 and ES-2 cells. The amount of hyaluronidase secreted to the conditioned medium of the cells was analyzed by Western blot using anti-hyaluronidase-1 and anti-hyaluronidase-2 antibodies. In accord with the higher activity of hyaluronidase (Fig. 3A), medium conditioned by ES-2 cells contained high levels of both hyaluronidase-l and hyaluronidase-2, whereas in OVCAR-3 conditioned medium both proteins were undetectable (Fig. 3H). Although ES-2 cells exhibited higher rate
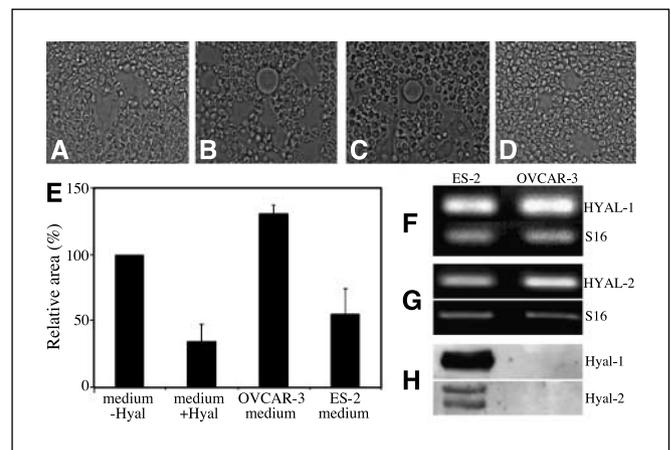
Figure 3. Expression, secretion, and biological activity of hyaluronidase by ovarian carcinoma ES-2 and OVCAR-3 cell lines. *A-E,* biological activity of hyaluronidase was measured using particle exclusion assay. The hyaluronan coat of chondrocytes was visualized by exclusion of fixed RBC. *A,* chondrocytes incubated in fresh medium. *B,* chondrocytes incubated with fresh medium and bovine testes hyaluronidase (0.3 mg/mL) for 15 to 30 minutes. *C* and *D,* chondrocytes incubated with medium conditioned by OVCAR-3 (*C*) or ES-2 (*D*). *E,* quantification of the relative hyaluronidase activity measured as the reduced area of the hyaluronan coat for (*A-D*). Activity of hyaluronidase was manifested by reduced area of the hyaluronan coat of chondrocytes due to its degradation. All the media that were tested were significantly different from each other ($n = 5$; two-tailed unpaired *t* test; $P < 0.05$), with the exception of medium + hyaluronidase and ES-2 medium. *F* and *G,* expression and secretion of hyaluronidase. Semiquantitative RT-PCR of mRNA levels of hyaluronidase-1 (*F*) and semiquantitative RT-PCR of mRNA levels of hyaluronidase-2 (*G*). S16 served as an internal control. *H,* Western blot analysis of hyaluronidase-1 and hyaluronidase-2 protein levels in the medium of OVCAR-3 and ES-2 cells.
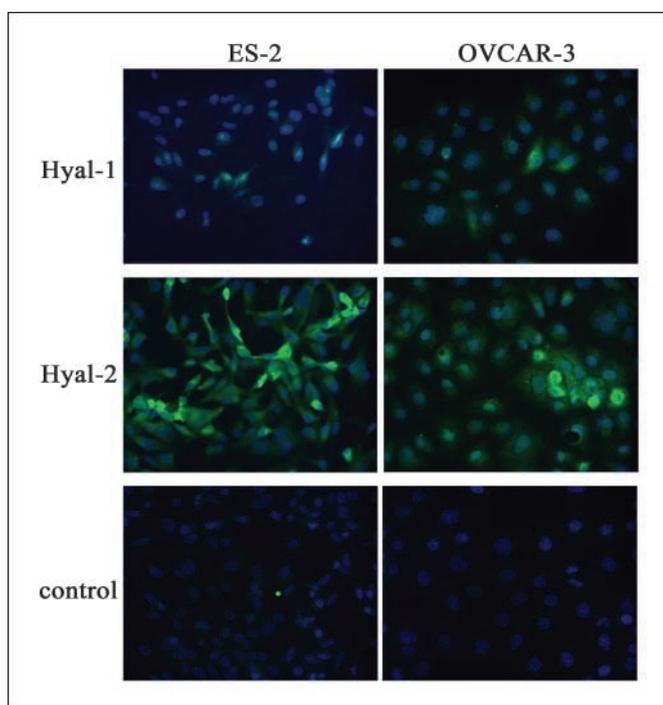
Figure 4. Immunofluorescence staining of hyaluronidase-1 and hyaluronidase-2 in human epithelial ovarian carcinoma cells. ES-2 (*left*) and OVCAR-3 (*right*) cells were incubated with anti-hyaluronidase-1 or anti-hyaluronidase-2 antibody (*green*). The cells nuclei were stained with DAPI (*blue*). Note the similar amount of intracellular hyaluronidases in the different cell lines.

of proliferation in 10% FCS, they showed decreased cell survival in serum-free medium relative to OVCAR-3 cells. Thus, conditioned medium was collected in most experiments 24 hours after serum removal, when both cell lines were viable. Traces of hyaluronidase-1 and hyaluronidase-2 could be detected in medium from OVCAR-3 cells by using double the amount of protein (data not shown).

Magnetic resonance imaging detection of hyaluronidase secreted by ovarian carcinoma cells. ES-2 and OVCAR-3 cells were grown to confluence in a 96-well plate for 24 hours. Hyaluronan-GdDTPA-beads (1 mg/mL) were added to the cells without changing the culture medium (DMEM + 10% FCS) such that the hyaluronidase secreted to the medium was not washed out.

Hyaluronidase expressed by tumor cells induced an elevation in R_1 and R_2 (Fig. 5). R_1 of fresh medium was 0.45 ± 0.04 s^{-1}, R_1 of OVCAR-3 medium was 0.47 ± 0.03 s^{-1}, and R_1 of ES-2 medium was 0.51 ± 0.04 s^{-1}. R_2 of fresh medium was 2.42 ± 0.06 s^{-1}, R_2 of OVCAR-3 medium was 2.48 ± 0.03 s^{-1}, and R_2 of ES-2 medium was 2.77 ± 0.01 s^{-1}. Therefore, ES-2 cells that showed high secretion of biologically active hyaluronidase in the particle exclusion assay (Fig. 3) also showed the higher increase in R_1 and R_2 relaxation rates (Fig. 5). We found significant difference in R_1 and R_2 between ES-2 and OVCAR-3 ($n = 3$; two-tailed unpaired t test; $P = 0.005$) and between ES-2 and the negative control ($n = 5$; two-tailed unpaired t test; $P = 0.0002$).

The change in relaxation rate of hyaluronan-GdDTPA-beads could be induced by hyaluronidase that was secreted to the medium and reacted with the contrast material to degrade it. Alternatively, the change could be attributed to hyaluronidase that was anchored to the cells surfaces (32). To differentiate between these two options, we repeated the experiment with the medium alone. Conditioned medium from ES-2 or OVCAR-3 cells was

depleted of residual cells by centrifugation and hyaluronan-GdDTPA-beads were added. This approach resulted in R_2 relaxation changes that were similar to those measured in the presence of cells. Hyaluronan-GdDTPA-beads suspended in conditioned medium of ES-2 cells showed larger increase in R_2 relative to that observed for OVCAR-3 cells ($n = 6$; two-tailed unpaired t test; $P < 0.0001$). Thus, the R_2 effect detected by MRI was consistent with the different levels of biologically active hyaluronidase secreted by these two human ovarian carcinoma cell lines.

***In vivo* detection of hyaluronidase by magnetic resonance imaging in ovarian carcinoma tumors.** To examine the feasibility of the new contrast material *in vivo*, we administered it s.c. through a catheter to the vicinity of s.c. ES-2 tumors in immunodeficient nude mice and compared the activation of the contrast material with that observed in the absence of tumor (Fig. 6). Regions of interest were selected in the area of contrast material enhancement. The most significant changes in R_1 and R_2 were observed at early time points between the time of injection and the next scan (after 2.5 minutes). The rapid dynamics were consistent with rapid activation of the contrast material detected *in vitro* (Fig. 2B).

Longitudinal R_1 relaxation maps revealed significant changes associated with activation of hyaluronan-GdDTPA-beads in the vicinity of the ES-2 tumors [high ΔR_1; $\Delta R_1 = R_1(t = 2.5 \text{ minutes}) - R_1(t = 0)$; four tumor-bearing mice and two control mice; $P = 0.01$ relative to control animal and 0.039 relative to area with contrast material near the tumor; two-tailed unpaired t test; Fig. 6E]. Activation of the contrast material was evident but smaller for R_2 relaxation [high ΔR_2; $\Delta R_2 = R_2(t = 2.5 \text{ minutes}) - R_2(t = 0)$; $P = 0.06$ relative to control area in the tumor-bearing mice and 0.078 relative to control mice without tumor; two-tailed unpaired t test; $n = 4$ in each experimental group].

Discussion

Molecular imaging aimed at detection of specific enzymatic reactions by MRI is a novel and exciting approach for noninvasive characterization of processes in living organisms (33). Previous agents developed for MRI analysis of enzymatic activity include
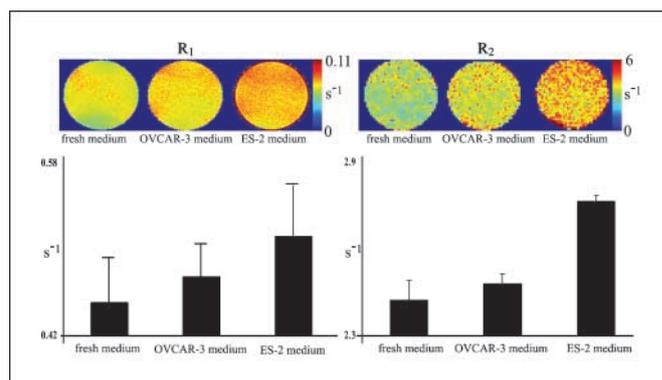
Figure 5. MRI detection of hyaluronidase secreted by ovarian carcinoma cells. ES-2 and OVCAR-3 human epithelial ovarian carcinoma cells were grown in 96-well plates. Hyaluronan-GdDTPA-beads (1 mg/mL) were added for 15 to 30 minutes. The R_1 and R_2 relaxation rates of the medium were measured by slice selective MRI, positioning the slice within the medium layer above the adhered cells. *Top,* representative color-coded maps of R_1 (*left*) and R_2 (*right*) derived for hyaluronan-GdDTPA-beads suspended in fresh medium (*left* in each map) or in conditioned medium collected from OVCAR-3 (*center* in each map) or ES-2 (*right* in each map) cells; *bottom, columns,* mean R_1 and R_2 relaxation rates from the respective samples ($n = 3$); *bars,* SD.
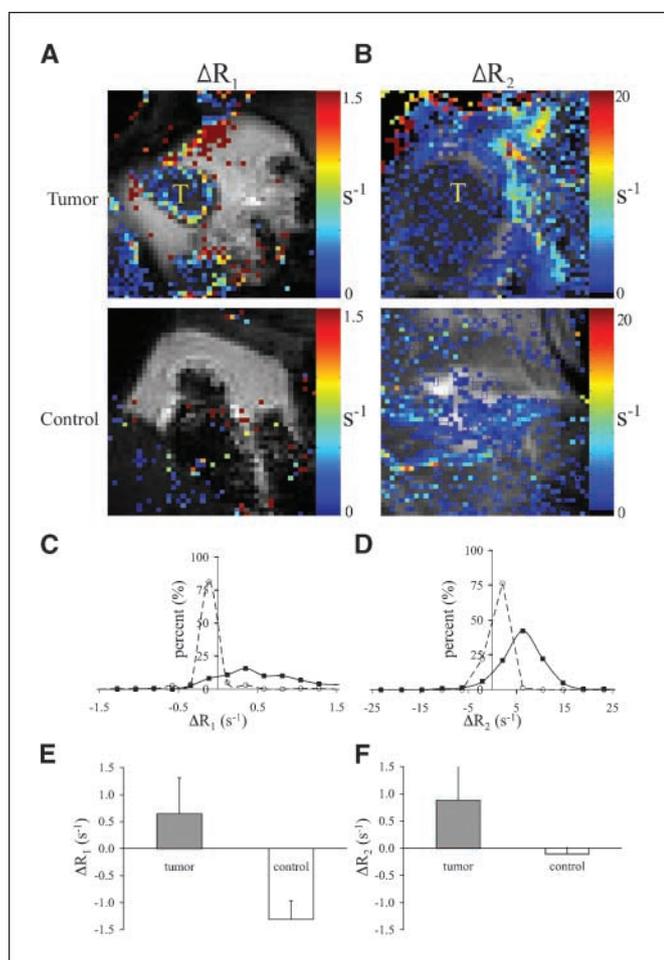
Figure 6. *In vivo* detection of hyaluronidase activity in ovarian carcinoma tumors. *A* and *B,* the early change in R_1 or R_2 relaxation rate after interstitial administration of the hyaluronan-GdDTPA-beads [$\Delta R = R(t = 2.5 \text{ minutes}) - R(t = 0)$; *color scale*] was overlaid on a spin echo MRI image [*gray scale*]. Hyaluronan-GdDTPA-beads were administered via a catheter to the hind limb in the vicinity of ES-2 tumor (*T*) or in a control mouse. R_1 or R_2 maps generated from multiecho spin echo MRI acquired immediately after contrast injection were subtracted from R_1 or R_2 maps taken 2.5 minutes after injection. *C* and *D,* histograms describing the distribution of the ΔR_1 and ΔR_2 in the vicinity of the contrast material injection. Those histograms were measured from the same animals shown in (*A* and *B*), respectively. Note the large positive ΔR_1 and ΔR_2 in tumor-bearing mice (■) relative to control mice (○). *E* and *F, columns,* average ΔR_1 and ΔR_2 in the areas of contrast material injection in all tumor-bearing and control mice; *bars,* SD. The differences between the control and the tumor groups were found to statistically significant for ΔR_1 (two-tailed unpaired *t* test; $P = 0.039$; four tumor-bearing mice and four control mice) but only close to significant for ΔR_2 (two-tailed unpaired *t* test; $P = 0.06$; four tumor-bearing mice and two control mice). Activation of the contrast material by hyaluronidase secreted by the ES-2 tumor resulted in positive ΔR_1 and ΔR_2 in the vicinity of the tumor rim, whereas in naive animals the contrast material was not activated and negative ΔR_1 and ΔR_2 values were measured in the injection area as expected for rapid clearance of the contrast material.

substrates for β-galactosidase (34), proteases (33, 35), and iron-binding proteins, such as tyrosinase (36), the transferrin receptor (37, 38), and ferritin (39). Some of these agents exploit the change in relaxivity that occurs on enzymatic activity, affecting the interaction of water molecules with the contrast material. The large number of mechanisms influencing magnetic relaxivity offers many possibilities for targeting different enzymatic reactions. The aim of the present work was to develop contrast material for detection of hyaluronidase, a key enzyme that alters the angiogenic balance of the extracellular matrix by mediating breakdown of antiangiogenic high molecular weight hyaluronan into its proangiogenic low molecular weight products.

We report here a single step assay for detection of hyaluronidase, which allows noninvasive *in vivo* imaging by MRI. Using beads enveloped with hyaluronan-GdDTPA, we were able to detect changes in R_1 and R_2 relaxation rates after addition of either hyaluronidase or conditioned medium taken from human ovarian carcinoma cell lines that express and secrete hyaluronidase. In the presence of hyaluronan-GdDTPA-beads, the relaxation rates increased significantly after interaction with hyaluronidase. The observed changes in relaxation rate can be due to degradation of hyaluronan-GdDTPA but can also be due to binding of hyaluronidase to the contrast material. Hypothetically, degradation of hyaluronan can cause a release of GdDTPA or low molecular weight hyaluronan-GdDTPA, which might allow increased interaction with water and affect MRI contrast. Similarly, binding of hyaluronidase to hyaluronan could change the conformation of hyaluronan and expose GdDTPA to water possibly by interfering with a direct interaction of the negatively charged carboxyl groups of hyaluronan with the free coordination sites of gadolinium.

The ability to detect physiologic levels of hyaluronidase by MRI using hyaluronan-GdDTPA-beads was tested *in vitro* using human epithelial ovarian carcinoma cells. The expression of hyaluronidase-1 and hyaluronidase-2 was evaluated in OVCAR-3 and ES-2 human ovarian carcinoma cell lines. Although no significant differences were found in the level of mRNA in the two cell lines, major difference was detected in the protein level of hyaluronidase-1 and hyaluronidase-2 secreted to the culture medium. ES-2 cells secreted high level of both hyaluronidases to the medium; on the contrary, both hyaluronidase-1 and hyaluronidase-2 were undetectable in OVCAR-3 cells medium.

The biological activity of hyaluronidase, as manifested in particle exclusion assay by degradation of the hyaluronan coat of chondrocytes, revealed that ES-2 cells not only secrete more hyaluronidase than OVCAR-3 cells but that the secreted hyaluronidase is also active. Remarkably, the new MRI contrast material reported here, hyaluronan-GdDTPA-beads, allowed detection of hyaluronidase when added to solution and also when secreted by the human ovarian carcinoma cells. Moreover, the contrast material was sensitive to the different levels of hyaluronidase between the two ovarian cell lines. The measured changes in R_1 and R_2 were consistent with the Western blot and particle exclusion assay, all of which showed higher levels of hyaluronidase in the medium of ES-2 cells. The R_1 and R_2 changes induced by bovine testes hyaluronidase were larger than those induced by conditioned medium of the ovarian carcinoma cells, reflecting probably the concentration of active enzyme, the type of enzyme (hyaluronidase-1 and hyaluronidase-2 relative to testis hyaluronidase, respectively), as well as other modulators of hyaluronidase activity that are secreted by the cells.

The ability to detect hyaluronidase activity *in vivo* was shown on s.c. ES-2 ovarian carcinoma tumors after s.c. administration of the contrast material in the tumor region. Due to rapid clearance of the contrast material after s.c. administration, activation of the contrast material was analyzed from the early increase in the relaxation rate measured from the first two time points after administration of the contrast material. A rapid increase in R_1 and R_2 relaxivities was detected in the periphery of the hyaluronidase-secreting tumor. The increased relaxivity induced by hyaluronidase could aid in detection of regions of enzyme activity. In the control regions and control mice, ΔR_1 and ΔR_2 were negative

(i.e., there was a decrease in relaxation rate, consistent with the lack of activation and the rapid clearance of the s.c. administered contrast material, in the absence of a tumor).

This approach opens new possibilities for the study of ovarian carcinoma-induced angiogenesis. We have reported previously that human epithelial ovarian cancer cells show gonadotropin regulation of both vascular endothelial growth factor (VEGF; ref. 40) and CD44, the cell surface receptor for hyaluronan (41). Thus, elevated level of luteinizing hormone and follicle-stimulating hormone as occurs at menopause can lead to increased adhesion of ovarian cancer cells on hyaluronan-coated surfaces in the peritoneum as well as augmented expression of VEGF. However, elevated expression of VEGF is insufficient for inducing angiogenesis in the presence of high molecular weight hyaluronan. This was shown previously in the preovulatory ovarian follicle, where we showed that hyaluronan serves as an antiangiogenic shield, protecting the oocyte from premature vascularization in the presence of elevated levels of VEGF (42). Secretion of hyaluronidase by ovarian carcinoma cells can allow micrometastases to overcome this barrier and induce vascularization.

This study provides *in vitro* proof-of-principle and *in vivo* demonstration for the ability to detect hyaluronidase activity by MRI. For ovarian cancer, i.p. administration would allow the contrast material to adhere to the external surface of small tumor nodules and be activated by secreted hyaluronidase, enabling detection of hyaluronidase on the cell surface and the hyaluronidase secreted to the pleural effusion. Due to the particular dissemination pattern of ovarian cancer, i.p. administration of targeted chemotherapy is being evaluated as a route that would increase tumor targeting and reduce systemic toxicity (43). The contrast material reported here would highlight tumors that have the capacity to adhere to the peritoneal wall and activate angiogenesis by overcoming the antiangiogenic effect of high molecular weight hyaluronan. Because tumor-derived hyaluronidase has been implicated in tumor invasion across the mesothelial cell layer, a noninvasive imaging of this enzyme at sites of tumor implantation may aid in defining the risk for spread beyond the peritoneal cavity.

Clearly, development of this approach for other *in vivo* applications and particularly for i.v. administration would require significant modification of the carrier beads to make them more compatible for administration. The size of the hyaluronan-GdDTPA complex and the rapid degradation of hyaluronan in circulation by plasma hyaluronidase-1 (7) may limit i.v. administration.

In summary, we show here a novel contrast material for noninvasive MRI detection of hyaluronidase. Hyaluronan-GdDTPA-beads can help decipher the role of hyaluronan and its breakdown products in regulation of angiogenesis during normal development and cancer progression. Specifically, we anticipate that this approach will facilitate visualization and thereby the study of the role of hyaluronidase in peritoneal metastatic dissemination of ovarian carcinoma.

Acknowledgments

References

1. Toole BP. Hyaluronan and its binding proteins, the hyaladherins. Curr Opin Cell Biol 1990;2:839–44.
2. Slevin M, Krupinski J, Kumar S, Gaffney J. Angiogenic oligosaccharides of hyaluronan induce protein tyrosine kinase activity in endothelial cells and activate a cytoplasmic signal transduction pathway resulting in proliferation. Lab Invest 1998;78:987–1003.
3. Stern R. Devising a pathway for hyaluronan catabolism: are we there yet? Glycobiology 2003;13:105–15R.
4. Balazs EA, Hogberg B, Laurent TC. The biological activity of hyaluron sulfuric acid. Acta Physiol Scand 1951;23:168–78.
5. Cobbin LB, Dicker SE. Some characteristics of plasma and urine "hyaluronidase." J Physiol (Paris) 1962;163:168–74.
6. Toole BP. Hyaluronan: from extracellular glue to pericellular cue. Nat Rev Cancer 2004;4:528–39.
7. Csoka AB, Frost GI, Stern R. The six hyaluronidase-like genes in the human and mouse genomes. Matrix Biol 2001;20:499–508.
8. Afify AM, Stern M, Guntenhoner M, Stern R. Purification and characterization of human serum hyaluronidase. Arch Biochem Biophys 1993;305:434–41.
9. Wei MH, Latif F, Bader S, et al. Construction of a 600-kilobase cosmid clone contig and generation of a transcriptional map surrounding the lung cancer tumor suppressor gene (TSG) locus on human chromosome 3p21.3: progress toward the isolation of a lung cancer TSG. Cancer Res 1996;56:1487–92.
10. Mio K, Carrette O, Maibach HI, Stern R. Evidence that the serum inhibitor of hyaluronidase may be a member of the inter-α-inhibitor family. J Biol Chem 2000;275:32413–21.
11. Novak U, Stylli SS, Kaye AH, Lepperdinger G. Hyaluronidase-2 overexpression accelerates intracerebral but not subcutaneous tumor formation of murine astrocytoma cells. Cancer Res 1999;59:6246–50.
12. Chang NS. Transforming growth factor-β1 blocks the enhancement of tumor necrosis factor cytotoxicity by hyaluronidase Hyal-2 in L929 fibroblasts. BMC Cell Biol 2002;3:8.
13. West DC, Hampson IN, Arnold F, Kumar S. Angiogenesis induced by degradation products of hyaluronic acid. Science 1985;228:1324–6.
14. Tamakoshi K, Kikkawa F, Maeda O, et al. Hyaluronidase activity in gynaecological cancer tissues with different metastatic forms. Br J Cancer 1997;75:1807–11.
15. Jones LM, Gardner MJ, Catterall JB, Turner GA. Hyaluronic acid secreted by mesothelial cells: a natural barrier to ovarian cancer cell adhesion. Clin Exp Metastasis 1995;13:373–80.
16. Carpenter PM, Dao AV. The role of hyaluronan in mesothelium-induced motility of ovarian carcinoma cells. Anticancer Res 2003;23:3985–90.
17. Casey RC, Oegema TR, Jr., Skubitz KM, Pambuccian SE, Grindle SM, Skubitz AP. Cell membrane glycosylation mediates the adhesion, migration, and invasion of ovarian carcinoma cells. Clin Exp Metastasis 2003;20:143–52.
18. Lessan K, Aguiar DJ, Oegema T, Siebenson L, Skubitz AP. CD44 and β1 integrin mediate ovarian carcinoma cell adhesion to peritoneal mesothelial cells. Am J Pathol 1999;154:1525–37.
19. Gardner MJ, Catterall JB, Jones LM, Turner GA. Human ovarian tumour cells can bind hyaluronic acid via membrane CD44: a possible step in peritoneal metastasis. Clin Exp Metastasis 1996;14:325–34.
20. Stern M, Stern R. An ELISA-like assay for hyaluronidase and hyaluronidase inhibitors. Matrix 1992;12:397–403.
21. Frost GI, Stern R. A microtiter-based assay for hyaluronidase activity not requiring specialized reagents. Anal Biochem 1997;251:263–9.
22. Vercruysse KP, Lauwers AR, Demeester JM. Kinetic investigation of the degradation of hyaluronan by hyaluronidase using gel permeation chromatography. J Chromatogr B Biomed Appl 1994;656:179–90.
23. Takahashi T, Ikegami-Kawai M, Okuda R, Suzuki K. A fluorimetric Morgan-Elson assay method for hyaluronidase activity. Anal Biochem 2003;322:257–63.
24. Cramer JA, Bailey LC. A reversed-phase ion-pair high-performance liquid chromatography method for bovine testicular hyaluronidase digests using postcolumn derivatization with 2-cyanoacetamide and ultraviolet detection. Anal Biochem 1991;196:183–91.
25. Nishida Y, Knudson CB, Nietfeld JJ, Margulis A, Knudson W. Antisense inhibition of hyaluronan synthase-2 in human articular chondrocytes inhibits proteoglycan retention and matrix assembly. J Biol Chem 1999;274:21893–9.
26. Gouin S, Winnik FM. Quantitative assays of the amount of diethylenetriaminepentaacetic acid conjugated to water-soluble polymers using isothermal titration calorimetry and colorimetry. Bioconjug Chem 2001;12:372–7.
27. Luo Y, Prestwich GD. Synthesis and selective cytotoxicity of a hyaluronic acid-antitumor bioconjugate. Bioconjug Chem 1999;10:755–63.
28. Cohen M, Klein E, Geiger B, Addadi L. Organization and adhesive properties of the hyaluronan pericellular coat of chondrocytes and epithelial cells. Biophys J 2003;85:1996–2005.
29. Straach KJ, Shelton JM, Richardson JA, Hascall VC, Mahendroo MS. Regulation of hyaluronan expression during cervical ripening. Glycobiology 2005;15:55–65.
30. Csoka AB, Scherer SW, Stern R. Expression analysis

of six paralogous human hyaluronidase genes clustered on chromosomes 3p21 and 7q31. Genomics 1999;60:356–61.

31. Ziv K, Nevo N, Dafni H, et al. Longitudinal MRI tracking of the angiogenic response to hind limb ischemic injury in the mouse. Magn Reson Med 2004; 51:304–11.

32. Rai SK, Duh FM, Vigdorovich V, Danilkovitch-Miagkova A, Lerman MI, Miller AD. Candidate tumor suppressor HYAL2 is a glycosylphosphatidylinositol (GPI)-anchored cell-surface receptor for jaagsiekte sheep retrovirus, the envelope protein of which mediates oncogenic transformation. Proc Natl Acad Sci U S A 2001;98:4443–8.

33. Bogdanov A, Jr., Matuszewski L, Bremer C, Petrovsky A, Weissleder R. Oligomerization of paramagnetic substrates result in signal amplification and can be used for MR imaging of molecular targets. Mol Imaging 2002;1:16–23.

34. Louie AY, Huber MM, Ahrens ET, et al. *In vivo* visualization of gene expression using magnetic resonance imaging. Nat Biotechnol 2000;18:321–5.

35. Zhao M, Josephson L, Tang Y, Weissleder R. Magnetic sensors for protease assays. Angew Chem Int Ed Engl 2003;42:1375–8.

36. Alfke H, Stoppler H, Nocken F, et al. *In vitro* MR imaging of regulated gene expression. Radiology 2003; 228:488–92.

37. Bremer C, Weissleder R. *In vivo* imaging of gene expression. Acad Radiol 2001;8:15–23.

38. Hogemann D, Ntziachristos V, Josephson L, Weissleder R. High throughput magnetic resonance imaging for evaluating targeted nanoparticle probes. Bioconjug Chem 2002;13:116–21.

39. Cohen B, Dafni H, Meir G, Harmelin A, Neeman M. Ferritin as an endogenous MRI reporter for noninvasive imaging of gene expression in C6 glioma tumors. Neoplasia 2005;7:109–17.

40. Schiffenbauer YS, Abramovitch R, Meir G, et al. Loss of ovarian function promotes angiogenesis in human ovarian carcinoma. Proc Natl Acad Sci U S A 1997;94:13203–8.

41. Schiffenbauer YS, Meir G, Maoz M, Even-Ram SC, Bar-Shavit R, Neeman M. Gonadotropin stimulation of MLS human epithelial ovarian carcinoma cells augments cell adhesion mediated by CD44 and by $\alpha(v)$-integrin. Gynecol Oncol 2002;84:296–302.

42. Tempel C, Gilead A, Neeman M. Hyaluronic acid as an anti-angiogenic shield in the preovulatory rat follicle. Biol Reprod 2000;63:134–40.

43. Cannistra SA. Cancer of the ovary. N Engl J Med 2004;351:2519–29.

Magnetic Resonance Imaging Visualization of Hyaluronidase in Ovarian Carcinoma

Liora Shiftan, Tomer Israely, Miriam Cohen, et al.

Updated version	Access the most recent version of this article at: http://cancerres.aacrjournals.org/content/65/22/10316

Cited articles	This article cites 42 articles, 8 of which you can access for free at: http://cancerres.aacrjournals.org/content/65/22/10316.full#ref-list-1
Citing articles	This article has been cited by 5 HighWire-hosted articles. Access the articles at: http://cancerres.aacrjournals.org/content/65/22/10316.full#related-urls

E-mail alerts	Sign up to receive free email-alerts related to this article or journal.
Reprints and Subscriptions	To order reprints of this article or to subscribe to the journal, contact the AACR Publications Department at pubs@aacr.org.
Permissions	To request permission to re-use all or part of this article, use this link http://cancerres.aacrjournals.org/content/65/22/10316. Click on "Request Permissions" which will take you to the Copyright Clearance Center's (CCC) Rightslink site.